2023 45th Annual International Conference of the IEEE Engineering in Medicine & Biology Society (EMBC) | 979-8-3503-2447-1/23/$31.00 ©2023 IEEE | DOI: 10.1109/EMBC40787.2023.10340624

How 3D scaffolds with different mechanical properties affect the activity of neuronal networks in *in vitro* models*

Francesca Callegari, Martina Brofiga, Mariateresa Tedesco, and Paolo Massobrio

***Abstract*— Three-dimensionality has been proven extensively to be critical in the development of a reliable model for different anatomical compartments and for many diseases. Currently, we can produce implantable structures that help in the regeneration of different tissues such as bone and heart. Different is the situation when we consider the neuronal compartment. As it is still difficult to understand exactly how the brain computes, to conceive how the complex chain of neuronal events can generate conscious behavior, a comprehensive and workable model of neuronal tissue still has to be found. In this perspective, in the present work, we developed and compared different 3D scaffolds to understand the effects produced by the mechanical and material properties of four different scaffolds on a 3D neuronal network. To help in preclinical testing procedure, the scalability and ease-of-use of the different approaches were also taken into consideration.**

***Clinical Relevance*— By comparing different 3D scaffolds for the creation of neuronal constructs, the results in this paper move towards understanding the best strategy to develop functional 3D neuronal units for reliable pre-clinical studies.**

I. Introduction

Currently, one treatment method for regenerating damaged tissues is implanting tissue engineered scaffolds [1]. Implantable 3D scaffolds can be used for reconstructing different anatomical defects while promoting the physiological restoration of different functional tissues [2]. In fact, cell behavior is critically influenced by the several cues they receive from their surrounding microenvironment, which is intrinsically three-dimensional [3]. In addition, cellular development, reactions, and protein expression are tightly dependent on the material and mechanical properties of the extracellular matrix (ECM) that is reproduced by scaffolds. An alteration of these factors is often linked to pathological conditions as well as the insurgence of cancer diseases [4]. The development of new materials (biomimetic polymeric compounds, hydrogels, etc.) and of new fabrication techniques (3D printing, bioprinting, etc.) already brought to different successful examples of what can be achieved with 3D implantable scaffolds. The most apparent examples are bone-aimed scaffolds [5]. Recent advances in soft tissues have produced workable models of heart tissue [6], liver [7], and auricle [8]. Reliable 3D scaffolds can help also with tumors, not only by loading implantable structures with drugs for delivering the right dosage directly on the site, with a consequent increase in the efficacy rate of treatments [9], but also for the *in vitro* modeling of the disease [10]. Conceptually, one of the most difficult tissues to tackle and reproduce is the nervous one as to this date it is still hard to understand how neuronal events (spikes, network bursts, oscillatory rhythms, etc.) give rise to a particular conscious experience, or to any conscious experience at all [11]. Therefore, a first problem to solve is understanding how the 3D cues given by the scaffold modify the insurgence of these neuronal events. One of the most common and classic scaffolds is the glass microbeads [12]. This synthetic scaffold is highly reproducible (in terms of obtained geometries and porosity); however, it lacks some of the fundamental mechanical characteristics of the native tissues. To better reproduce these properties of the extracellular matrix, different hydrogels have been tested. The advancements in natural biomaterials were accompanied with the development new techniques that involve their use, like bioprinting, which has been studied for example in the development of regeneration devices and for spinal cord injury repair [13], [14]. These techniques greatly improve the reproducibility of the scaffold, but they do not yet achieve the high resolution necessary for the creation of the fine structures of the neural tissues. From this point of view, synthetic polymers can achieve greater results. Recently, a molding technique was employed to create a PDMS 3D scaffold that successfully reproduced a traumatic brain injury (TBI) [15]. Later in 2021, Koroleva and coworkers developed a 3D scaffold with a very precise laser technique to support the long-term culturing of functional neuronal networks [16]. Others have focused on reproducing the porosity of the extracellular matrix. Sponge-like structures were created with different materials, like PDMS [17], polyurethane-PLGA [1], and silk-collagen [18]. In the present work, we developed and directly compared different kinds of scaffolds in the effect they produced on the electrophysiological activity of neuronal networks recorded by means of Micro-Electrode Arrays (MEAs). Our findings showed that sponge-like materials made of PDMS produce effects comparable to the ones found with hydrogels, which have mechanical properties similar to the extracellular matrix, and commented on the reproducibility, efficacy and scalability of the methods.

II. Materials and Methods

A. 3D cell cultures with different scaffolds

The experimental protocol aimed at reducing the number of sacrificed animals and minimize their suffering and was

*Research (partially) supported by Fondazione Link (Compagnia di San Paolo).

F. C. is with the University of Genova, Department of Informatics, Bioengineering, Robotics and Systems Engineering (DIBRIS), Genova, 16145, Italy (corresponding author, phone: +39 3490800668, email: francesca.callegari@edu.unige.it).

M. B. is with the University of Genova, Department of Informatics, Bioengineering, Robotics and Systems Engineering (DIBRIS), Genova, 16145, Italy (email: martina.brofiga@dibris.unige.it). She is co-founder and CTO of ScreenNeuroPharm s.r.l, Sanremo, 18038, Italy.

M. T. is with the University of Genova, Department of Informatics, Bioengineering, Robotics and Systems Engineering (DIBRIS), Genova, 16145, Italy (email: mariateresa.tedesco@unige.it).

P. M. the University of Genova, Department of Informatics, Bioengineering, Robotics and Systems Engineering (DIBRIS), Genova, 16145, Italy (email: paolo.massobrio@unige.it).

approved by the European Animal Care Legislation (2010/63/EU), by the Italian Ministry of Health in accordance with the D.L. 116/1992 and by the guidelines of the University of Genova (Prot. 75F11.N.6JI, 08/08/18).

Cells were plated on 60-electrode Micro-Electrode Arrays (Multi Channel Systems, MCS, Reutlingen, Germany) to record their electrophysiological activity. The device was dry oven sterilized at 120 ºC for 3 h. Then, the surface was coated (overnight at 37 ºC) with Poly-L-Ornithine at 100 $\frac{\mu g}{ml}$ and rinsed with sterile water. Cortical tissues were collected from Sprague-Dawley rat embryos at gestational day 18 (E18). They were digested with an enzymatic solution of Trypsin at 0.125% and DNAse (Sigma-Aldrich) at 0.03% (diluted in Hanks' solution). The process was quenched after 20 min at 37◦C with a 10 % FBS solution. Tissues were mechanically dissociated with a fine-tipped Pasteur pipette. Single cells were suspended in culture medium made up of Neurobasal Medium (Sigma-Aldrich), Glutamax at 1% (Sigma-Aldrich), B-27 supplement at 2% (Sigma-Aldrich), penicillin-streptomycin solution at 1% (Sigma-Aldrich). For every 3D configuration, it was necessary to create a monolayer of cells tightly coupled to the surface serving as interface between the 3D cell culture and the recording electrodes. Following standard protocols, cortical cells were plated directly onto the active area of the MEA at the final cell density of 1'800 $\frac{cells}{mm^2}$. To ensure the adhesion of the monolayer, cells were incubated for at least 3 hours before adding the 3D scaffold. After the creation of the 3D culture (details below for the pipelines to follow for the different scaffolding methods), cultures were maintained in the incubator that guaranteed a controlled atmosphere of 37 ºC, 5% CO_2, and 95% humidity for about 3 weeks. Half the volume of the medium was replaced first at day *in vitro* (DIV) 5, and then twice a week, with BrainPhys™ (Stemcell Technologies) neuronal medium, supplemented with 2% NeuroCult™ SM1 Neuronal Supplement (Stemcell Technologies), 1% penicillin-streptomycin solution (Sigma-Aldrich), and 1% Glutamax (Sigma-Aldrich).

Thermogels scaffolds

Two different thermogels were tested. For both, the setting-up procedure is the same (Fig. 1A), except for the final concentration of the cells that depended on the specifics indicated by the product itself. Briefly, ECM gel (Sigma-Aldrich) is prepared from mice Engelbreth-Holm-Swarm sarcoma and contains a mixture of laminin, collagen type IV, heparin sulfate proteoglycan, entactin (and other minor components, final protein concentration of 8-12 $\frac{mg}{ml}$, which can be diluted 1:2). It will undergo thermally activated polymerization when brought to 20-40°C. Geltrex™ LDEV-Free Reduced Growth Factor Basement Membrane Matrix (ThermoFisher Scientific) is a comparable soluble basement membrane from murine EHS tumors, free of viruses including lactose dehydrogenase elevating virus (LDEV), but with concentration of 12-18 $\frac{mg}{ml}$ (which can be diluted 2:3). Apart from the different dilution factors, the pipeline for cell seeding is the same as follows. After the consolidation of the monolayer, the medium was removed to ensure excessive medium gel dilution. Working on ice, single cells that were stored in the incubator were mixed uniformly in the gels (following the different dilution factors). Then, the gel-cell solution was added on the MEAs and stored in the incubator for at least 2 hours to allow a proper polymerization before adding culture medium.

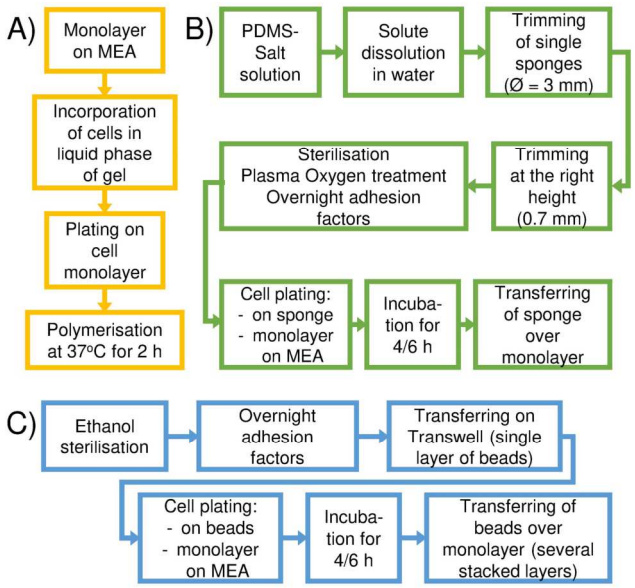

Figure 1: Schematics of the pipeline for the creation of different types of 3D scaffolds. (A) Thermogel scaffolds. (B) PDMS sponge scaffold. (C) Glass microbeads scaffolds.

PDMS sponge scaffold

The PDMS sponges were created adapting the protocol in [18] (Fig. 1B). They need to be created at least a week before cell preparation. First, NaCl was sieved to obtain granules with a size inferior to 600 µm. A PDMs solution (curing agent 1:10 w/w in prepolymer) was poured into a Petri dish, then the selected salt was added and mixed in to obtain a uniform layer. The Petri was then put in a vacuum pump to ensure the removal of any air bubble and cured in dry oven at 80 ºC for 30 minutes. After removing the polymerized mixture from the dish, the top/bottom excessive layer (if present) was trimmed. The compound was placed in a beaker with distilled water for 72 hours to leach out the salt. The water was changed 2-3 times per day. Then, scaffolds were cut out with a biopsy punch (Ø = 3 mm) and trimmed to height with an *ad hoc* 3D-printed mold. The 3D scaffolds were then stored in deionized water and autoclaved (wet cycle, 121 °C, 20 min). After, the scaffolds underwent plasma oxygen treatment (100 W for 60 seconds) and coated with Poly-L-Ornithine at 100 $\frac{\mu g}{ml}$ (overnight at 37 ºC). On the day of cell preparation, the 3D sponges were rinsed with sterile water and then with culture medium. The cell suspension was then seeded on top of the scaffold (about 700 k cells, considering that about 30% of the cells will be lost). The seeded sponge was moved to the incubator for at least 5 hours to ensure a strong cellular adhesion. Then, the scaffolds were moved onto the cell monolayers, incubated for an additional hour and flood with culture medium.

Glass microbeads scaffold

The day before cell retrieval, glass microbeads (Thermo Fisher) with a 40 µm diameter (certified mean diameter of 42.3 ± 1.1 µm) were sterilized in 70% Ethanol for 3 hours (Fig. 1C). After rinsing with sterile water (3 times), the adhesion factor solution was added and left at 37ºC overnight.

The day of the dissection, the microbeads were again rinsed and then moved to a Transwell® (Ø = 33 mm^2), where they self-assembled into a single uniform layer. The hexagonal geometrical structure allowed determining the number of beads necessary to cover the porous membrane (~20'000) and the total exposed surface available for cell seeding (~80 mm^2). To facilitate cell seeding, each Transwell® was submerged in culture medium. Dissociated cells were then plated into the Transwell® taking into consideration two factors: (i) when transferred to the MEA, about 25% cells were lost; (ii) a fraction of cells will never fall on the membrane and will not come in contact with the microbeads. The Transwell® was then incubated for about 6 hours to ensure a strong enough adhesion of the cells to the glass surface to allow transferring them. Then, several layers of seeded microbeads were sequentially stacked over the monolayer of cells previously created on the MEA surface. Overall, 4/5 layers of seeded beads were placed in the culturing area. To ensure the survival of cells, a drop (500 μl) of culture medium was added to the culture overnight. The following day, the overall structure was stable enough for the addition of the rest of the medium for long-term culturing (1 ml). The protocol was adapted from [19].

B. Data collection and analysis

We recorded the extracellular activity of the 3D cultures when the networks reached a mature stage of development at DIV 18. The electrophysiological activity was acquired with the MEA2100 system (Multi Channel Systems, Reutlingen, Germany) with a sampling frequency of 10 kHz. The raw data was used to extract the spiking activity with the adaptive method presented in [20]. Briefly, the algorithm uses a different threshold set independently for each channel, computed as 8 times the standard deviation of the signal biological and thermal noise, the peak lifetime period, and the refractory period to extract the spike trains. Then, bursts were detected with the string method described in [21] by setting at 5 the minimum number of spikes in a burst and at 100 ms the maximum inter spike interval within a burst. The spiking and bursting activity were characterized in terms of the following parameters: (i) Mean Firing Rate (MFR) i.e., the mean number of spikes per second averaged over the active channels (sp/s); (ii) Mean Bursting Rate (MBR) i.e., the corresponding value for burst (bursts/min); (iii) the Spike per Bursts (SpXBst) i.e., the average number of spikes in each burst; (iv) the Percentage of Random Spiking (%rnd) i.e., the fraction of spikes that do not pertain to a burst. A channel was considered active if its MFR was greater than 0.1 sp/s, and bursting if its MBR was greater than 0.4 bursts/min. All the algorithms were developed in Matlab (The Mathworks, Natik, US). Since data do not follow a normal distribution (Kolmogorov-Smirnov normality test) Statistical analysis was performed by means of a nonparametric Kruskal–Wallis test using Origin (Origin Lab Northampton, Ma), with significance set at $p < 0.05$.

III. Results

In view of a serialization of the use of the scaffolds, their usability needs to be considered. One of the most common 3D protocols, based on glass microbeads, has the disadvantage of requiring a very long and technical cell seeding procedure (6 hours + 12 hours to allow settling down and adding medium). On this behalf, the easiest in terms of cell seeding are the thermogels (5 hours), which however are more problematic then the previous in terms of yield, as the specimen loss over time is higher (the gels tend to detach from the surface more easily than the set beads construct). About the PDMS sponges, they have to be custom made, but from a single preparation several scaffolds can be obtained. Then, the pipeline for cell seeding is straightforward (6 hours), the application on the cell monolayer being the only step of the process to be completed with more attention in order to avoid the loss of a sample. Moreover, compared to glass microbeads, a more efficient sterilization can be employed.

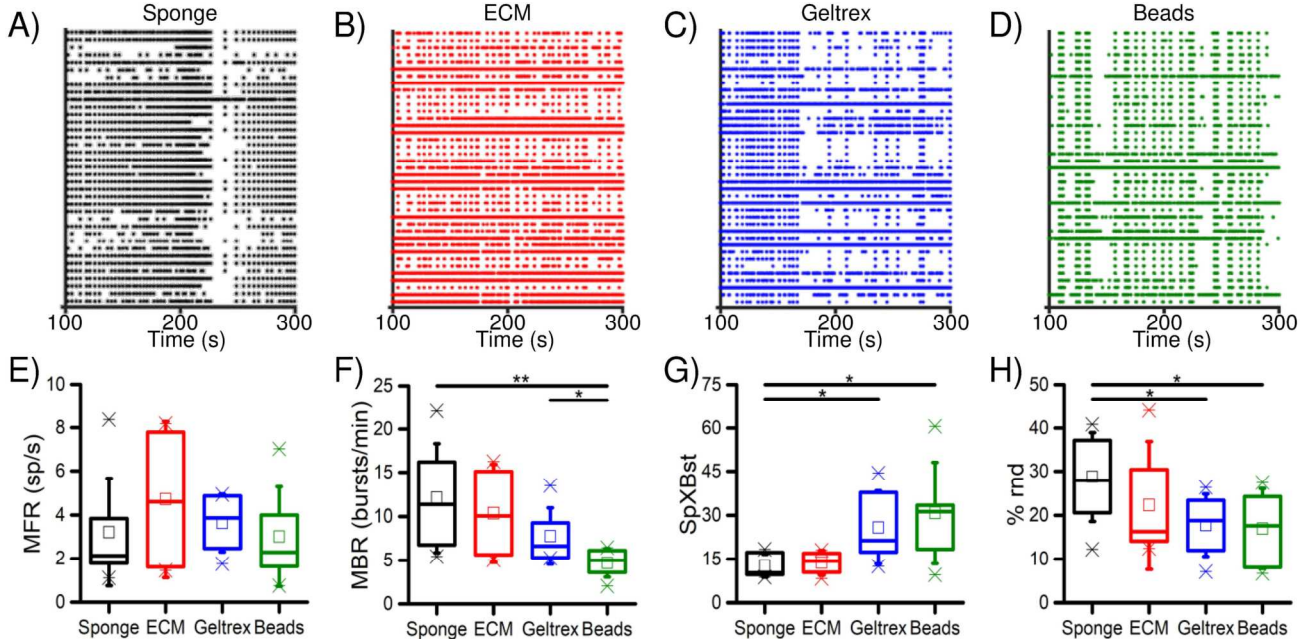

Figure 2. Spiking and bursting activity. 200-second raster plots of a representative (A) sponge, (B) ECM gel, (C) Geltrex, and (D) glass microbeads cultures. (E) Mean Firing Rate, (F) Mean Bursting Rate, (G) Spike per Burst, (H) Percentage of random spiking of 6 networks for each configuration recorded at DIV 18 (* refers to $0.01 < p < 0.05$, ** to $p < 0.01$; Kruskal–Wallis non-parametric test)

Then, we investigated the effect of the different topological organization determined by the four presented scaffolds on the electrophysiological activity of the *in vitro* model (n = 6 samples for each configuration for reproducibility). For all the configurations, the dynamics of 3D cortical assemblies was characterized by the presence of both random spikes and synchronized bursts (Fig. 2A-D). All the configurations display a similar spiking activity, as demonstrated by the comparable values of MFR (Fig. 2E). However, the different kinds of scaffolds gave rise to a different temporal distribution of the events. In particular, the different spatial distribution of cells and mechanical properties of their environment brought to differences to arise in the frequency (Fig. 2F) and in the "density" of the bursts (Fig. 2G) with a consequent redistribution of the random spiking activity (Fig. 2H). Sponges present values of MBR that are comparable to those of the gels (especially the ECM gel). These MBR values were statistically higher than those obtained with glass microbeads. In this configuration, the bursts resulted to be denser, i.e., made up by a higher number of spikes then the other configurations, especially if compared to the sponge values, as a statistical difference was found. A similar behavior was found in the case of the Geltrex. In these two configurations, in fact, the activity resulted to be more organized, and consequently less random spiking was detected. Additionally, it is worth noticing that that all these results were constant over time. In fact, from DIV 18, all the scaffolds were able to maintain stable these parameters for the next weeks.

IV. Conclusion

In the present work, we analyzed the differences in the electrophysiological activity of 3D neuronal networks brought by the peculiar mechanical and material properties of four scaffolds (n = 6 samples for each for reproducibility). We found the highest dissimilarities when comparing the beads scaffold with sponges, that on the contrary seem to induce an effect on the recorded activity similar to one of the gels, and in particular of the ECM gel. This result might suggest comparable mechanical properties of the two scaffolds. In perspective, further analyses need to be carried out to detect which intrinsic parameters give rise to the peculiar patterns of electrophysiological activity in order to select the ones that are better suited for a workable model of the neuronal tissue. Further advances should also include other critical elements of the brain, such as modularity (i.e., the peculiar topological organization of the brain in different modules) and heterogeneity (i.e., the coexistence of different neuronal types), or embed also the blood-brain barrier (BBB), an essential feature for both drug testing and to study the etiology of diseases [22]. Finally, it is worth noticing that the electrophysiological activity of the entire 3D network was recorded only from the layer directly coupled on the planar MEA surface, therefore the observable information is limited compared to the analyzed system. For this reason, the coupling of the 3D scaffold to the recording electrode is of great importance. Some evidence (like the number of active electrodes and the amplitude of the recorded signal) suggested that some of the scaffolds produce a better coupling to the electrodes.

References

[1] B. Du *et al.*, "A waterborne polyurethane 3D scaffold containing PLGA with a controllable degradation rate and an anti-inflammatory effect for potential applications in neural tissue repair," *J. Mater. Chem. B*, vol. 8, no. 20, pp. 4434–4446, May 2020, doi: 10.1039/D0TB00656D.

[2] M. P. Nikolova and M. S. Chavali, "Recent advances in biomaterials for 3D scaffolds: A review," *Bioact. Mater.*, vol. 4, pp. 271-292, Oct. 2019, doi: 10.1016/J.BIOACTMAT.2019.10.005.

[3] M. Hippler *et al.*, "3D Scaffolds to Study Basic Cell Biology," *Adv. Mat.,* vol. 31, no. 26, Feb. 2019, Art. no. 1808110, doi: 10.1002/adma.201808110.

[4] C. Bonnans, J. Chou, and Z. Werb, "Remodelling the extracellular matrix in development and disease," *Nat. Rev. Mol. Cell Biol.*, vol. 15, no. 12, pp. 786–801, Nov. 2014, doi: 10.1038/nrm3904.

[5] C. Lin *et al.*, "Advances in Filament Structure of 3D Bioprinted Biodegradable Bone Repair Scaffolds," *Int. J. Bioprinting*, vol. 7, no. 4, pp. 43–64, Oct. 2021, doi: 10.18063/IJB.V7I4.426.

[6] R. J. Jabbour *et al.*, "In vivo grafting of large engineered heart tissue patches for cardiac repair," *JCI Insight*, vol. 6, no. 15, Aug. 2021, Art. no. e144068, doi: 10.1172/JCI.INSIGHT.144068.

[7] G. Mazza *et al.*, "Decellularized human liver as a natural 3D-scaffold for liver bioengineering and transplantation," *Sci. Reports*, vol. 5, no. 1, pp. 1–15, Aug. 2015, doi: 10.1038/srep13079.

[8] J. Yin *et al.*, "3D-printed high-density polyethylene scaffolds with bioactive and antibacterial layer-by-layer modification for auricle reconstruction," *Mater. Today Bio*, vol. 16, Dec. 2022, Art. no. 100361, doi: 10.1016/J.MTBIO.2022.100361.

[9] W. Dang *et al.*, "Implantable 3D Printed Hydrogel Scaffolds Loading Copper-Doxorubicin Complexes for Postoperative Chemo/Chemodynamic Therapy," *ACS Appl. Mater. Interfaces*, vol. 15, no. 4, pp. 4911-4923, Jan. 2023, doi: 10.1021/ACSAMI.2C18494.

[10] C. Fischbach *et al.*, "Engineering tumors with 3D scaffolds," *Nat. Methods*, vol. 4, no. 10, pp. 855–860, Sep. 2007, doi: 10.1038/nmeth1085.

[11] R. Adolphs, "The unsolved problems of neuroscience," *Trends Cogn. Sci.*, vol. 19, no. 4, pp. 173-175, Apr. 2015, doi: 10.1016/J.TICS.2015.01.007.

[12] M. Brofiga *et al.,* "Three-dimensionality shapes the dynamics of cortical interconnected to hippocampal networks," *J. Neural Eng*, vol. 17, no. 5, Oct. 2020, Art. no. 56044, doi: 10.1088/1741-2552/abc023.

[13] D. Joung *et al.*, "3D Printed Neural Regeneration Devices," *Adv. Funct. Mater.*, vol. 30, no. 1, Jan. 2020, Art. no. 1906237, doi: 10.1002/ADFM.201906237.

[14] T. Bedir *et al.*, "3D bioprinting applications in neural tissue engineering for spinal cord injury repair," *Mater. Sci. Eng. C*, vol. 110, May 2020, Art. no. 110741, doi: 10.1016/J.MSEC.2020.110741.

[15] C. Chen *et al.*, "Develop a 3D neurological disease model of human cortical glutamatergic neurons using micropillar-based scaffolds," *Acta Pharm. Sin. B*, vol. 9, no. 3, pp. 557–564, May 2019, doi: 10.1016/J.APSB.2019.03.004.

[16] A. Koroleva *et al.*, "In vitro development of human iPSC-derived functional neuronal networks on laser-fabricated 3D scaffolds," *ACS Appl. Mater. Interfaces*, vol. 13, no. 7, pp. 7839–7853, Feb. 2021, doi:10.1021/ACSAMI.0C16616/.

[17] S. Bosi *et al.*, "From 2D to 3D: Novel nanostructured scaffolds to investigate signalling in reconstructed neuronal networks," *Sci. Rep.*, vol. 5, no. 1, pp. 1–11, Apr. 2015, doi: 10.1038/srep09562.

[18] Y. T. L. Dingle *et al.*, "Functional Characterization of Three-Dimensional Cortical Cultures for In Vitro Modeling of Brain Networks," *iScience*, vol. 23, no. 8, Aug. 2020, Art. no. 101434, doi: 10.1016/j.isci.2020.101434.

[19] M. Tedesco *et al.*, "Interfacing 3D Engineered Neuronal Cultures to Micro-Electrode Arrays: An Innovative In Vitro Experimental Model," *J. Vis. Exp.*, vol. 2015, no. 104, Oct. 2015, Art. no. e53080, doi: 10.3791/53080.

[20] A. Maccione *et al.*, "A novel algorithm for precise identification of spikes in extracellularly recorded neuronal signals," *J. Neurosci. Methods*, vol. 177, no. 1, pp. 241–249, 2009, doi: 10.1016/j.jneumeth.2008.09.026.

[21] M. Chiappalone *et al.*, "Burst detection algorithms for the analysis of spatio-temporal patterns in cortical networks of neurons," *Neurocomputing*, vol. 65–66, pp. 653–662, Jun. 2005, doi: 10.1016/j.neucom.2004.10.094.

[22] M. Brofiga and P. Massobrio, "Brain-on-a-Chip: Dream or Reality?," *Front. Neurosci.*, vol. 16, Mar. 2022, Art. no. 837623, doi: 10.3389/FNINS.2022.837623.